The Journal of the Acoustical Society of America

Acoustic radiation force on a parametrically distorted bubble

--Manuscript Draft--

Manuscript Number:	JASA-02137R1
Full Title:	Acoustic radiation force on a parametrically distorted bubble
Short Title:	Radiation force
Article Type:	Regular Article
Corresponding Author:	Alexey Maksimov, Doctor of Science in Physics and Mathematics Pacific Oceanological Institute Vladivostok, Primorye RUSSIAN FEDERATION
First Author:	Alexey Maksimov, Doctor of Science in Physics and Mathematics
Order of Authors:	Alexey Maksimov, Doctor of Science in Physics and Mathematics
	Timothy Grant Leighton, Professor
Section/Category:	Physical Acoustics
Keywords:	radiation force; bubbles; Faraday waves; ultrasonic cleaning
Abstract:	The subject of acoustic radiation pressure on a gas bubble is important in many applications because it controls how bubbles are moved by acoustic fields to target locations, and often how they act upon the target. Previous theoretical treatments assume a spherical bubble undergoing linear pulsations, but some (such as cleaning using Faraday waves on the bubble wall) require that the bubble be aspherical. Therefore, this paper derives ways to calculate the variation in the radiation pressure due to the non-spherical bubble oscillations. The magnitude and direction of the radiation force are determined by two factors: the amplitude of volume oscillations, V_{m}, and the phase relationship between those oscillations and the acoustic field which drives them. There are two key findings that correct for the predictions of a model accounting for only linear pulsations. First, the growth of the radiation force slows down as V_{m} ceases to increase linearly with increasing amplitude of the acoustic wave above the threshold. Second, although both models show that the direction of the force relative of the standing wave antinode can be attractive or repulsive depending on frequency, when distortion modes are included the frequency at which this force changes its sign is shifted.

Acoustic radiation force on a parametrically distorted bubble

A. O. Maksimov*

Pacific Oceanological Institute, Far Eastern Branch of the Russian Academy of Sciences, Vladivostok, 690041 Russia

T. G. Leighton

Institute of Sound and Vibration Research, Faculty of Engineering and the Environment, University of Southampton, Highfield, Southampton SO17 1BJ, UK

(Dated: November 30, 2017)

Abstract

The subject of acoustic radiation pressure on a gas bubble is important in many applications because it controls how bubbles are moved by acoustic fields to target locations, and often how they act upon the target. Previous theoretical treatments assume a spherical bubble undergoing linear pulsations, but some (such as cleaning using Faraday waves on the bubble wall) require that the bubble be aspherical. Therefore, this paper derives ways to calculate the variation in the radiation pressure due to the non-spherical bubble oscillations. The magnitude and direction of the radiation force are determined by two factors: the amplitude of volume oscillations, V_m, and the phase relationship between those oscillations and the acoustic field which drives them. There are two key findings that correct for the predictions of a model accounting for only linear pulsations. First, the growth of the radiation force slows down as V_m ceases to increase linearly with increasing amplitude of the acoustic wave above the threshold. Second, although both models show that the direction of the force relative of the standing wave antinode can be attractive or repulsive depending on frequency, when distortion modes are included the frequency at which this force changes its sign is shifted.

PACS numbers: PACS: 43.25.Yw, 43.30.Es, 43.35.Ei

Keywords: radiation force; bubbles; Faraday waves; ultrasonic cleaning

* maksimov@poi.dvo.ru; Corresponding author.

I. INTRODUCTION

The acoustic radiation force exerted by a plane or a spherical wave on a compressible sphere in a non-viscous fluid has been extensively investigated over the last six decades. The effects of particle compressibility on the radiation force were initially studied by Yosioka et al. [1] Subsequently, Gor'kov [2] used a fluid dynamics approach to derive formulae for the general radiation force exerted on a particle by a plane wave and any stationary acoustic wave. Eller [3] was the first to calculate the radiation force on a small bubble. A refined version of Eller's result has been obtained by Lee and Wang [4]. All of these studies were based on the model of an ideal fluid that ignores the processes of viscosity and thermal conductivity. In many situations, this idealization is acceptable. Calculation of the radiation force in a real fluid requires addressing not only the linearized equations of motion for momentum, density, energy and entropy, but also the so-called equations of acoustic streaming, which represent time-averaged equations of motion, taken up to the quadratic terms in the amplitude of the perturbation [5]. Since streaming can cause a bubble or particle to change location, it is particularly important to assess its potential to do this if the acoustic field is being used to move bubbles/particles by radiation forces. A complete solution to this problem was given by Doinikov [5–8]. Viscous and thermal effects become important when the size of the bubble becomes comparable to the acoustic boundary layers (thermal and viscous) [9].

If a gas bubble of radius R_0 in a liquid of sound speed c_0 is driven by an acoustic wave of low circular frequency ω, (such that $\omega R_0/c_0 << 1$), then at all amplitudes of that driving wave the bubble undergoes a spherically-symmetric wall oscillation (i.e. a breathing mode pulsation). However, if the amplitude of the driving waves exceeds a well-defined threshold, then the nonlinear response of the gas bubble results in parametrically-generated shape oscillations, superimposed upon the pulsation. The study of the consequences of parametrically excited bubble responses and associated energy and gas flow began in the 1970s [10, 11]. Above the critical driving pressure threshold, which is minimal at the resonance of the breathing mode, regular patterns of stationary surface waves are observed on the bubble wall [12–21]. The theory for the pattern formation on the bubble wall has been derived in recent studies [22–24].

The acoustic radiation force is caused by the transference of momentum flux from an imposed oscillatory pressure field (which has zero amplitude at pressure nodes; and maximum amplitude at pressure antinodes) to a bubble (noting that the term 'bubble' consists not just of the ball of gas – which provides this oscillatory system with stiffness – but also the surrounding liquid, which provides the vast majority of the inertia). The additional channel of energy absorption due to the generation of surface modes alters the transference of momentum flux and thus modifies the radiation force. The influence of the parametric response on the radiation force on a bubble was observed by Asaki & Marston [25], but this effect was avoided for the purpose of comparing the measured radiation force (by way of equilibrium location) with radiation force theory. The measured free decay of quadrupole oscillations of large bubbles acoustically trapped in water [26] demonstrated a standing capillary wave roughening. Asaki & Marston [26] also described the associated energy flow "out of" a particular bubble mode as a consequence of the roughening, and suggested that the observed anomalous damping might result from nonlinear coupling [27].

Interest in Faraday waves has increased in recent years because of a range of applications, including ultrasonic foggers [28] and, hypothetically, in the generation of the alligator 'water dance' [29]. This theoretical study was designed to support a new ultrasonic cleaning technique, the Ultrasonically Activated Stream (UAS) [30, 31]. UAS achieves cleaning with cold water streams at flow rates of ~ 1 litre min^{-1}, generating zero-to-peak acoustic pressure at the surface to be cleaned of less than 100 kPa. The basic principle is that water is fed into a hollow horn that contains an ultrasonic transducer operating in excess of 100 kHz. UAS systems clean by non-inertial cavitation, whereby the ultrasound stimulates surface waves on the bubble wall. These in turn create shear and greatly enhance the cleaning efficiency of water at the interface. The ultrasound and microbubbles in the flow both travel down the stream of water to the target that is to be cleaned. If the bubbles are ultrasonically activated when they are on the target, the cleaning ability of the liquid is enhanced in three ways: the bubbles are attracted to the surface to be cleaned by Bjerknes radiation forces, and are not as rapidly washed away by the flow as they would be in the absence of ultrasound; the bubbles are particularly attracted into crevices by secondary Bjerknes radiation forces; such crevices are traditionally more difficult to clean by wiping or brushing; surface waves on the walls of the bubble, excited by the ultrasound, produce enhanced convection in the liquid and enhanced shear in the contaminant, causing its removal.

It is important to quantify the radiation forces that steer the bubbles towards the surface to be cleaned, and into crevices and other structures which are traditionally difficult to clean using brushes or wipes (which fail to penetrate crevices), or chemical methods (where the penetration of the chemical into the crevice is diffusion controlled). This not only because the action of these radiation forces place the surface waves and the local shear they cause in the proximity of the contaminant in the crevice, so that the surface waves can physically remove them. It is also because the translation of bubbles (with convection-inducing surface waves from the bulk liquid into the crevice) can enhance any chemical cleaning or disinfectant effects. If chemicals are added to the bulk liquid, then motion of the bubbles convects chemicals into the crevice, causing greater concentrations there than would be generated by diffusion alone [30, 32]. In this way, the same cleaning can be achieved in crevices using lower concentrations of chemicals in the bulk liquid, which have environmental, cost and safety implications. In this way UAS has successful achieved, using cold water,

- the cleaning of brain tissue and prions from surgical steel, the removal of contaminating material from bone transplants [33];
- the removal of biofilms of dental bacteria [33, 34];
- the cleaning of human skin [30, 32] and skin models [33, 35];
- the cleaning of marine biofoulant [36];
- the cleaning of railway track [37];
- the cleaning of hands, kitchen surfaces, tools, glue from jar labels, contaminated tubes, grease, salad and components of railway locomotives [30, 32, 38].

Clearly, the ability of radiation forces to resist buoyancy and turbulence and so move the bubble to the surface that is to be cleaned, and to enable it to penetrate crevices, is key to the ability of UAS to clean. To design the device with the ability to do this, it is important to be able to quantify the effect of surface waves on the radiation forces in order to calculate the parameters (frequency, bubble size, acoustic amplitude etc.) that will allow the radiation forces to overcome buoyancy, flow and turbulence. In this paper, we have made a step in the description of the physical processes that underlie this method. We have gained an understanding of how the presence of surface waves modifies the radiation pressure. The answer to the question of whether this change in the radiation force might be optimized, if at all, to enhance the cleaning results when a bubble hosting surface waves is located close to target surface to be cleaned is a topic for future research.

II. PHYSICAL MODEL

Assume that the size of the bubble is much smaller than the wavelength of sound, and then within this long wavelength limit, consider the case of weak dissipation. Dissipation is considered to be low if the bubble radius R_0 is large compared with the viscous δ_v and thermal δ_{th} wavelengths. The bubble is assumed to be centered in the origin of the coordinate system. We will consider only time-harmonic acoustic waves with an angular frequency ω, whose potential φ are of the form $\varphi(\boldsymbol{r})\exp(-\mathrm{i}\omega t)$, $\varphi(\boldsymbol{r}) = \varphi_{in}(\boldsymbol{r}) + \varphi_{sc}(\boldsymbol{r})$, where subindexes "in" and "sc" denote the contribution of the incident and scattered waves. The space-time dependence of the velocities $\boldsymbol{u}$ of the incident and scattered waves are $\boldsymbol{u}_{in,sc} = Re\left[\nabla\varphi_{in,sc}\exp(-\mathrm{i}\omega t)\right]$. As regards the externally imposed oscillatory pressure field wave, we shall consider a plane standing wave with the velocity potential given by $\varphi_{in} = \varphi_m \cos\left[\mathrm{i}\left(\boldsymbol{k}\cdot\boldsymbol{r} + kd\right)\right]\exp(-\mathrm{i}\omega t)$, where $\boldsymbol{k}$ is the wave vector, $\boldsymbol{r}$ is the position vector, and d is the shortest distance between the equilibrium center of the bubble and the nearest plane of the velocity node (or pressure antinode).

Acoustic waves give rise to a radiation-stress tensor [2]:

$$S_{ij} = -\left(P - P_\infty\right)\delta_{ij} - \rho_0 u_i u_j, \tag{1}$$

where P is the pressure in the presence of the sound and P_∞ is the constant static pressure that would, if the bubble was not present, exist in the liquid at the location currently occupied by the center of the bubble, and where ρ_0 is the constant mean density of the liquid. The integral of $-S_{ij}n_j$ over the bubble surface Σ_b is the force F_i, acting on the inclusion (here $\boldsymbol{n}$ is the normal). The static acoustic radiation force on a bubble could be simply calculated from the far-field integral over any spherical surface Σ enclosing the bubble [4]:

$$F_i = -\int_\Sigma \left[\langle P - P_\infty\rangle n_i + \rho_0 \langle u_i u_j\rangle n_j\right] d\Sigma, \tag{2}$$

where $\boldsymbol{n} = -\boldsymbol{e}_r$ on Σ and $\boldsymbol{n} = \boldsymbol{e}_r$ on Σ_b; the time averaging over a wave cycle is denoted by $\langle ... \rangle$. The mean momentum change in the surrounding fluid vanishes, since an ideal fluid cannot absorb momentum (no dissipation). The size of the bubble is assumed to be smaller than the acoustic wavelength, thus, there is, effectively, an "inner" region around the bubble, which may be regarded as incompressible. Far from the bubble, where nonlinear terms are

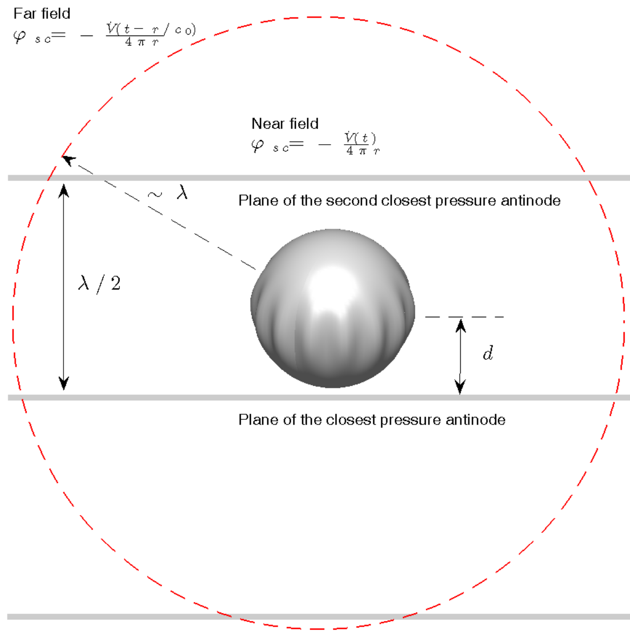

FIG. 1. (Color online) Schematic of a parametrically distorted bubble in the field of a standing acoustical wave φ_{in} of the frequency ω with d being the distance between the equilibrium center of the bubble and the nearest plane of the velocity nodes (or pressure antinodes). The size of the bubble is assumed to be smaller than the acoustic wavelength λ, thus, there is a region around the bubble, which may be regarded as incompressible.

small, the linear wave equation for the potential should be used. It is clear that "far from the bubble" means at distances $r \geq c_0T = \lambda$ ($T = 2\pi/\omega$), whereas "near the bubble" means at distances on the order of $0 \leq (r - R_0)/R_0 \approx 1$ or less. At distances large compared with R_0, though still small compared with the characteristic wavelength λ, one can find a general form of the solution for the scattered potential φ_{sc} by using the fact that φ_{sc} must decrease with increasing distance [39]:

$$\varphi_{sc}(\boldsymbol{r}, t) = -\frac{\dot{V}(t)}{4\pi r}, \tag{3}$$

where $V(t)$ is the volume of the bubble. In general, the total long-wave solution contains the contribution of the dipole term. For a gas bubble near the resonance, however, this dipole term is small [8]. At distances $r >> \lambda$, (i.e. in the "wave region"), φ_{sc} must represent an outgoing wave, i.e. must have the form [5]:

$$\varphi_{sc}(\boldsymbol{r}, t) = -\frac{\dot{V}(t - r/c_0)}{4\pi r}. \tag{4}$$

The pressure of a time-harmonic wave of angular frequency ω is given in terms of the potential function by $P(\boldsymbol{r}) = \mathrm{i}\rho_0\omega\varphi(\boldsymbol{r})$. To second order, $\langle P - P_\infty \rangle$ in Eq. (2) is finite and given by [4]:

$$\langle P - P_\infty \rangle = \frac{1}{2}\frac{\rho_0}{c_0^2}\left\langle \left(\frac{\partial\varphi}{\partial t}\right)^2 \right\rangle - \frac{1}{2}\rho_0 \left\langle |\nabla\varphi|^2 \right\rangle, \tag{5}$$

which is the minus time-average of the Lagrangian density.

The radiation force Eq. (2) is a bi-linear combination of two components: a spherically symmetric component $\varphi_{sc}(r)$, describing the scattered field [Eq. (4)] and the plane standing wave $\varphi_{in}(\boldsymbol{r}, t)$. The terms only associated with the incident field may be omitted since the radiation force vanishes in the absence of the bubble. The radiation force for an arbitrary sound field, in terms of momentum transport in the far field which involves the interaction of the incident and scattered fields and the flux associated with the scattered field, has the form [40]:

$$\boldsymbol{F} = \frac{\rho_0 k^2 r^2}{2}\int Re\left[\left(\frac{\mathrm{i}}{k}\frac{\partial\varphi_{in}}{\partial r}\varphi_{sc}^*\right) - \varphi_{sc}\varphi_{sc}^*\right]\boldsymbol{n}d\Omega, \tag{6}$$

where $d\Omega$ is the solid angle element ($d\Sigma = r^2 d\Omega$).

For the plane standing wave φ_{in}, the interference terms between the external field and the scattered wave are dominant and we have:

$$\boldsymbol{F} = -\boldsymbol{k}\frac{\rho_0\omega\varphi_m V_m \sin\alpha_V}{2}\sin(2kd), \tag{7}$$

where V_m is the amplitude and α_V is the phase of the component of the volume, oscillating with the frequency ω: $V \approx V_m \cos(\omega t + \alpha_V)$. Note that because we consider non-linear effects, other components will be present in the spectrum of the volume oscillations, but these components will have a relatively small magnitude. The expression for the radiation force on an air bubble Eq. (7) coincides with the commonly used form [3, 41, 42].

In the case of standing waves, when the wavelength exceeds the size of the bubbles and scattering is weak, the radiation force exerted by the standing wave is larger than that for the plane traveling wave [2]. In this case, in the quadratic expression for the force Eq. (2) the interference terms between the standing and scattered waves are significant, while for the traveling wave the transference of momentum by the wave is determined only by the scattered sound.

III. VARIATION OF THE BUBBLE VOLUME ABOVE THE THRESHOLD FOR INSTABILITY OF THE DISTORTION MODES

Within the framework of the adopted approximations, the radiation force on a bubble (6) depends on its volume pulsations. Above the threshold of parametric instability, volume pulsations and surface modes form a system of coupled oscillations. In our case, the problem is reduced to the analysis of the behavior of the bubble in a domain which is small compared with the wavelength where the liquid is incompressible and the amplitude of the imposed pressure field is constant.

The surface mode parametrically excited will be the one whose own natural frequency ω_l (where l is the order of the distortion mode) is closest to the subharmonic of the pump frequency, i.e. the mode for which $\omega_l \approx \omega/2$. The driving acoustic pressure which excites a surface mode will have a minimum (at the base of the U-shaped graph of acoustic pressure against frequency that maps out the threshold for the generation of surface waves [15, 43]) at a frequency close to the breathing mode resonance $\omega \approx \omega_0$ (where $\omega_0(R_0)$ is the natural frequency of the breathing mode). The threshold conditions to excite a mode, and its form in steady state, have been discussed widely at the end of past century [16, 17, 44–48].

In describing the regular patterns of surface waves which are observed on the bubble wall above the driving pressure threshold for shape oscillations, we follow the results of our earlier study [24]. We use the spherical coordinates (r, ϑ, α) where r is the radial displacement, and ϑ and α are the polar and azimuthal angles. The origin coincides with the center of the bubble. The equation of the bubble surface is $r = R_0 + \xi(\vartheta, \alpha, t)$.

An analysis of the behavior of the unsteady potential flows of the liquid in a spatial region D with a free surface S can be reduced to a treatment of the surface dynamics. Within this formalism, the shape of the surface S and the boundary potential at this surface Φ are the dynamical variables determining the state of the system [49]. Transition to the canonical variables $\xi(\vartheta, \alpha, t)$, $\Pi(\vartheta, \alpha, t) = -\rho_0 \left(R_0 + \xi(\vartheta, \alpha, t)\right) \Phi(\vartheta, \alpha, t)$ provides the simplest way to describe the nonlinear bubble dynamics [49]. Expansion of the variables in a series of spherical harmonics Y_{lm}:

$$\xi(\vartheta, \alpha, t) = \sum_{l=0}^{\infty} \sum_{m=-l}^{l} \xi_{lm}(t) Y_{lm}(\vartheta, \alpha), \quad \Pi(\vartheta, \alpha, t) = \sum_{l=0}^{\infty} \sum_{m=-l}^{l} \Pi_{lm}(t) Y_{lm}(\vartheta, \alpha) \tag{8}$$

can be used to diagonalize the quadratic Hamiltonian [49]:

$$
\begin{aligned}
H_0 &= \omega_0 a_{00}^* a_{00} + \sum_{m=-1}^{1} \frac{\Pi_{1m}^* \Pi_{1m}}{\rho_0 R_0^3} + \sum_{l=2}^{\infty} \omega_l \sum_{m=-l}^{l} a_{lm}^* a_{lm}, \\
\Pi_{lm} &= -\frac{\mathrm{i}}{\sqrt{2}} \left(\frac{\rho_0 R_0^3 \omega_l}{(l+1)} \right)^{1/2} \left(a_{lm} - (-1)^m a_{lm}^* \right), \\
\xi_{lm} &= \frac{\mathrm{i}}{\sqrt{2}} \left(\frac{\rho_0 R_0^3 \omega_l}{(l+1)} \right)^{-1/2} \left(a_{lm} + (-1)^m a_{lm}^* \right), \\
\Pi_{00} &= -\frac{\mathrm{i}}{\sqrt{2}} \left(\frac{\rho_0 R_0^3 \omega_l}{(l+1)} \right)^{1/2} \left(a_{00} - a_{00}^* \right), \\
\xi_{00} &= \frac{\mathrm{i}}{\sqrt{2}} \left(\frac{\rho_0 R_0^3 \omega_l}{(l+1)} \right)^{-1/2} \left(a_{00} + a_{00}^* \right),
\end{aligned} \tag{9}
$$

where $\omega_0 = \sqrt{3\gamma \left(P_\infty + 2\sigma/R_0\right) \left(\rho_0 R_0^2\right)^{-1}}$ is the frequency of the monopole pulsations ($l = 0$), γ is the polytropic exponent and σ is the surface tension. The quadratic Hamiltonian (8) also demonstrates the existence of the dipole modes ($l = 1$) corresponding to the translational motions; and the shape oscillations ($l \geq 2$), which have the form of surface capillary waves propagating over the surface of the bubble at the frequency $\omega_l = \sqrt{\sigma \left(l+1\right) \left(l+2\right) \left(l-1\right) \left(\rho_0 R_0^3\right)^{-1}}$.

The slowly varying complex amplitudes of the breathing $\tilde{a}_{00} = a_{00} \exp\left(\mathrm{i}\omega_0 t\right)$ and distortion modes $\tilde{a}_{lm} = a_{lm} \exp\left(\mathrm{i}\omega_l t\right)$ satisfy the equations that have the form [24]:

$$
\begin{aligned}
\frac{d\tilde{a}_{00}}{dt} &= \left[\mathrm{i}\left(\omega - \omega_0\right) - \gamma_0\right] \tilde{a}_{00} - \mathrm{i} C_{ll0} \sum_{m=-l}^{l} (-1)^m \tilde{a}_{lm}^* \tilde{a}_{l-m} + \frac{\sqrt{\pi} R_0^2 P_m}{\left(2\rho_0 R_0^3 \omega_0\right)^{1/2}}, \\
\frac{d\tilde{a}_{lm}}{dt} &= \left[\mathrm{i}\left(\omega/2 - \omega_l\right) - \gamma_l\right] \tilde{a}_{lm} - 2\mathrm{i} C_{ll0} (-1)^m \tilde{a}_{00} \tilde{a}_{l-m}^* \\
&\quad + 2 C_{n'll} \sum_{m'=-n'}^{n'} (-1)^{m'} \overline{Y_{n'm'} Y_{l-m} Y_{lm-m'}} \tilde{a}_{n'm'} \tilde{a}_{lm-m'}^*, \\
C_{ll0} &= \left(2^7 \pi\right)^{-1/2} \left(4l - 1\right) \omega_l \left(\rho_0 \omega_0 R_0^3\right)^{-1/2} R_0^{-1},
\end{aligned} \tag{10}
$$

where $\overline{A} = (4\pi)^{-1} \int A \sin\vartheta \, d\vartheta \, d\alpha$ and $P_m = \rho_0 \omega \varphi_m \cos(kd)$ $\left(P_{in}|_{\mathbf{r}=0} = \rho_0 \omega \varphi_m \cos(kd) \sin(\omega t)\right)$. The damping of the breathing mode, γ_0, and of the distortion modes of order l, γ_l, are included in the current model. It is assumed that thermal and viscous lengths are smaller than the bubble radius which is an evident restriction for the selected model. A detailed study of the damping mechanisms for surface modes in the general case (accounting for the presence of a viscous boundary layer) has been presented in Ref. [26], one of the few (if not only) places where such damping is directly measured for the $l = 2$ distortion mode of bubble oscillations.

In this study, we consider the simplest pattern – rolls [24]. This pattern is formed by two waves (ll) and $(l-l)$ (see Fig. 1) which form a sectoral harmonic. The shape of the surface oscillations on the sphere, described by sector harmonics, is a direct analogy of the roll structure observed on a parametrically distorted flat surface. This type of pattern has been well studied, so using a name that emphasizes the analogy with a well-known object seems justified. The resonant triads ($l + l \rightleftharpoons n'$) determine the type of pattern that manifests itself. These triads are formed by two unstable surface waves having the same frequency ω_l interacting to generate a wave of higher frequency $\omega_{n'} \approx 2\omega_l$. For the selected pattern (rolls), resonance triads, forming this state, have a negligible effect on the standing-wave amplitude of the rolls [24]. For this reason, we do not present the cumbersome expression for the coupling coefficient in the energy of interaction of the distortion modes $C_{n'll}$ or the equation for the amplitude of the high-frequency partner of the unstable mode $\tilde{a}_{n'm'}$ in the resonant triad. The complete system of canonical equations for the amplitudes and the description of the individual terms are contained in the file entitled 'supplementary_materials_1.pdf' that is contained within the Electronic Supplement [50].

The system of Eqs. (10) can be significantly simplified near the threshold of parametric instability which occurs when one of the eigenvalues of the linear stability analysis:

$$\lambda_{\pm} = -\gamma_l \pm \left\{ \frac{P_m^2 (4l-1)^2}{16^2 \rho_0^2 R_0^4 \Delta_0} - (\omega_l - \omega/2)^2 \right\}^{1/2}, \tag{11}$$

passes through zero at:

$$P_{th} = \frac{16\rho_0 R_0^2}{(4l-1)} \sqrt{\Delta_0 \Delta_l}, \quad \Delta_0 = \left[(\omega_0 - \omega)^2 + \gamma_0^2 \right], \quad \Delta_l = \left[(\omega_l - \omega/2)^2 + \gamma_l^2 \right]. \tag{12}$$

Above the threshold:

$$\begin{gathered} P_m = P_{th} + \Delta P, \quad P_{th} >> \Delta P_{th} \geq 0, \\ \lambda_+ \approx \frac{\Delta P}{P_{th}} \frac{\Delta_l}{\gamma_l}, \quad \lambda_- \approx -2\gamma_l - \frac{\Delta P}{P_{th}} \frac{\Delta_l}{\gamma_l}, \end{gathered} \tag{13}$$

we can reduce the description by eliminating the "fast" variables [22, 51]. From the mathematical point of view, we study the local bifurcations of vector field $y = (\tilde{a}_{00}, \tilde{a}_{ll}, \tilde{a}_{l-l})$ occurring in the neighborhood of a fixed point. The stationary states (fixed points) occur when the right hand sides of equations (9) become zero. The dynamical system for the rolls is of fifth order and there are three fixed points [22]. Figure 1 of Ref. [22] demonstrates the characteristics of the bifurcation diagram in the plane of the control parameters $(\omega/2\pi, P_m)$.

The solution to the system of equations (10) is based on the use of the master-slave principle known in applied mathematics as center-manifold reduction [52]. Near the point where the dynamical system of equations (10) loses its linear stability (in our case this occurs at the threshold), one can reduce the dimensionality of the system and exclude the stable variables (i.e. those that decay to the central manifold on timescales determined by the corresponding eigenvalues). Thus, if we are interested in long-time behavior, we need only to investigate the system restricted to the central manifold which is determined by a relatively simple equation.

The breathing mode and the high-frequency (stable) distortion mode n' are fast-phased in order to draw energy from the pumping and unstable modes l:

$$\begin{aligned}\tilde{a}_{00} = \frac{2\mathrm{i}(-1)^l C_{ll0}}{[\mathrm{i}\,(\omega-\omega_0)-\gamma_0]}\tilde{a}_{ll}\tilde{a}_{l-l} - \frac{\sqrt{\pi}R_0^2\,(P_{th}+\Delta P)}{(2\rho_0 R_0^3\omega_0)^{1/2}\,[\mathrm{i}\,(\omega-\omega_0)-\gamma_0]},\\ \frac{d\tilde{a}_{ll}}{dt} = [\mathrm{i}\,(\omega/2-\omega_l)-\gamma_l]\,\tilde{a}_{ll} - 2\mathrm{i}C_{ll0}(-1)^l\tilde{a}_{00}\tilde{a}^*_{l-l},\\ \frac{d\tilde{a}^*_{l-l}}{dt} = [-\mathrm{i}\,(\omega/2-\omega_l)-\gamma_l]\,\tilde{a}^*_{l-l} + 2\mathrm{i}C_{ll0}(-1)^l\tilde{a}^*_{00}\tilde{a}_{ll}.\end{aligned} \tag{14}$$

We can ignore the contribution of the high-frequency distortion mode n' for the rolls patterns [24]. The linear combination of $\tilde{a}_{ll}$ and $\tilde{a}^*_{l-l}$ corresponding to the eigenvalue λ_- also rapidly relaxes onto the central manifold, which leads to the formation of a standing wave in the azimuthal angle. Components, spreading in both clockwise and anti-clockwise directions, have equal absolute complex amplitudes:

$$\tilde{a}^*_{l\mp l} = -(-1)^l e^{\mathrm{i}(\phi_1+\phi_2)}\tilde{a}_{l\pm l}, \quad \sin\phi_1 = (\omega_l-\omega/2)\,\Delta_l^{-1/2}, \quad \sin\phi_2 = -\gamma_0\Delta_0^{-1/2}. \tag{15}$$

Thus, near the threshold, it is possible to rewrite the system of equations (10) in terms of the slowly varying standing-wave amplitude [24]:

$$
\begin{aligned}
&\frac{dB_{ll}}{dt} = \lambda_+ B_{ll} - 2\Gamma_0 \left(B_{ll}^* B_{ll}\right) B_{ll}, \\
&B_{ll} = \frac{1}{2\mathrm{i}} \left[\tilde{a}_{ll} e^{\mathrm{i}(\phi_2-\phi_1)/2} - (-1)^l \tilde{a}_{l-l}^* e^{-\mathrm{i}(\phi_2-\phi_1)/2}\right] = -\mathrm{i}\frac{\gamma_l}{\sqrt{\Delta_l}} e^{\mathrm{i}(\phi_1+\phi_2)/2} \tilde{a}_{ll}, \\
&\qquad\qquad\qquad\qquad \Gamma_0 = \frac{2\Delta_l}{\Delta_0 \gamma_l^3} C_{ll0}^2 \left[\gamma_0\gamma_l - (\omega/2-\omega_l)(\omega-\omega_0)\right],
\end{aligned}
\tag{16}
$$

The stationary solution, which we are interested in, has the form:

$$
B_{ll}^* B_{ll} = \frac{\lambda_+}{2\Gamma_0} = \frac{\Delta P}{P_{th}} \frac{\Delta_0 \gamma_l^2}{4C_{ll0}^2 \left[\gamma_0\gamma_l - (\omega/2-\omega_l)(\omega-\omega_0)\right]}. \tag{17}
$$

The next step is to calculate the variation of the bubble volume:

$$
\begin{aligned}
V - V_0 &= \int d\Omega \left[\frac{(R_0+\xi)^3}{3} - \frac{R_0^3}{3}\right] = V_0 \left[3\frac{\overline{\xi}}{R_0} + 3\frac{\overline{\xi^2}}{R_0^2} + \frac{\overline{\xi^3}}{R_0^3}\right] \\
&\approx 3V_0 \Bigg[\frac{1}{\sqrt{8\pi}\left(\rho_0 R_0^5 \omega_0\right)^{1/2}} \left(a_{00} + a_{00}^*\right) + \frac{1}{8\pi\rho_0 R_0^5 \omega_0} \left(a_{00}+a_{00}^*\right)^2 \\
&\quad + \frac{(l+1)}{8\pi\rho_0 R_0^5 \omega_l} \sum_{m=-l}^{l} \left(a_{lm} + (-1)^m a_{l-m}^*\right)\left(a_{lm}^* + (-1)^m a_{l-m}\right)\Bigg].
\end{aligned}
\tag{18}
$$

The term describing the volume pulsations at the frequency ω, which contributes to the radiation force after averaging over time, has the following form:

$$
\begin{aligned}
(V-V_0)_\omega = V_m \cos(\omega t + \alpha_V) = 3V_0 \Bigg[&\frac{1}{\sqrt{8\pi}\left(\rho_0 R_0^5 \omega_0\right)^{1/2}} \left(\tilde{a}_{00} e^{-i\omega t} + \tilde{a}_{00}^* e^{i\omega t}\right) + \\
&+ \frac{(l+1)(-1)^l}{4\pi\rho_0 R_0^5 \omega_l} \left(\tilde{a}_{ll}\tilde{a}_{l-l} e^{-i\omega t} + \tilde{a}_{ll}^* a_{l-l}^* e^{i\omega t}\right)\Bigg].
\end{aligned}
\tag{19}
$$

Substituting in this equation the explicit form of $\tilde{a}_{00}$ (see Eq. (13)) and expressing $\tilde{a}_{l\pm l}$ in terms of B_{ll}, we obtain:

$$
\begin{aligned}
(V-V_0)_\omega = 3V_0 \Bigg[&-\frac{(P_{th}+\Delta P)}{2\rho_0 R_0^2 \omega_0 \sqrt{\Delta_0}} \sin(\omega t + \phi_2) \\
&+ \frac{(4l-1)\omega_l \Delta_l B_{ll}^* B_{ll}}{8\pi\rho_0 R_0^5 \omega_0 \sqrt{\Delta_0}\gamma_l^2} \cos(\omega t + \phi_1 + 2\phi_2) \\
&+ \frac{(l+1)}{2\pi\rho_0 R_0^5 \omega_l} \frac{\Delta_l B_{ll}^* B_{ll}}{\gamma_l^2} \cos(\omega t + \phi_1 + \phi_2)\Bigg].
\end{aligned}
\tag{20}
$$

The expressions in the second and third lines of Eq. (19) have a similar structure, but vary considerably in magnitude near the resonance size $\sqrt{\Delta_0} << \omega_0$. The term in the second line is due to the resonance coupling between the distortion and monopole modes and contains a large resonant factor $\omega_0/\sqrt{\Delta_0} >> 1$. By contrast, the term in the third line describes a simple quadratic effect on the amplitude of the distortion modes and can be neglected. Substituting the explicit expression for the $B^*_{ll}B_{ll}$ (Eq. (17)), we obtain:

$$(V - V_0)_\omega = 3V_0 \frac{8\sqrt{\Delta_l}}{(4l-1)\omega_0} \cos\left[\omega t + \phi_2 + \pi/2 - \frac{\Delta P}{P_{th}} \cot(\phi_1 + \phi_2)\right],$$
$$V_m = V_0 \frac{24\sqrt{\Delta_l}}{(4l-1)\omega_0}, \qquad \alpha_V = \phi_2 + \pi/2 - \frac{\Delta P}{P_{th}} \cot(\phi_1 + \phi_2). \tag{21}$$

Therefore it follows from this equation that, close to the threshold of the parametric instability, the amplitude of the volume oscillation, V_m, remains constant despite increases in the driving pressure, and remains equal to the value it took at the threshold. The interaction of this mode with the parametrically unstable surface waves leads only to variations in the phase relationship between the bubble pulsations and the phase of the driving field.

Such behavior is experimentally confirmed by a series of studies [13–15] in which the two-frequency method has been used for high-resolution bubble sizing. In this technique, in addition to a pumping wave the bubble is insonified by a high frequency imaging wave. For applications with millimeter-sized bubbles, the pumping frequency is of kilohertz order, whilst the imaging frequency is usually around a megahertz. Because of the great difference between the timescales associated with these two fields, the slow oscillations of the bubble wall, having frequency ω_0, ω_l ($\omega_0 \approx 2\omega_l$), will modulate the scattering imaging wave. Ramble *et al.* [15] have discovered that there exists a significant difference in the transient times taken to establish steady-state subharmonic and fundamental combination frequency signals (the so-called "ring-up" times). The signal corresponding to the excitation of the fundamental combinative components remains constant during the (long) transition period during which the parametrically unstable surface modes grow to attain their stationary amplitudes. This indicates that the interaction with the surface modes does not change the amplitude of the radial pulsations and causes only a phase shift.

To take a deeper view at the manifestations of the derived solution, one needs to consider an approach based on the use of partial wave scattering functions, $s_l = \exp(\eta_l)$, $\eta_l = \delta_l + i\gamma_l$ [53, 54] in terms of which the scattering amplitude is expressed (here l denotes the index of the spherical harmonic in the expansion of the scattering amplitude). Consider Eq. (28b) of

Ref. [53], where the LHS are terms in the standard standing-wave radiation force series while the RHS shows that the effect of modal damping (gamma) is not limited to that specific mode: thus, for example, the combined damping of the $l = 0$ and $l = 1$ modes (monopole and dipole modes) alter the radiation force contribution of the $l = 0$ mode. As an illustration of this approach, we evaluated the s-partial wave scattering function [55]. However, since only the first term $l = 0$ of this expansion (s-scattering) is taken into account in this paper, the simplifications that this approach provides will be used in the subsequent development of the results presented: this is relevant for a more complex structure of the external field, beyond the resonance condition of driving field and for the bubble located close to the boundary where there is an effective coupling between monopole and higher multipole modes [53, 54].

IV. DISCUSSIONS

The influence of the bubble dynamics above the threshold of parametric instability on the magnitude and direction of the radiation force Eq. (7) depends on two factors: V_m and $\sin\alpha_V$. As shown above, the first difference in the behavior of the radiation force above the threshold (compared to its behavior below the threshold) is that the amplitude of volume oscillations, V_m, ceases to increase linearly with increasing amplitude of the acoustic wave and has a constant value.

Let us describe the impact of the second factor, $\sin\alpha_V$, that can be presented in the following form:

$$\begin{aligned}\sin\alpha_V &= \sin\left[\phi_2 + \pi/2 - \frac{\Delta P}{P_{th}}\cot\left(\phi_1+\phi_2\right)\right]\\ &= \frac{1}{\sqrt{\Delta_0}}\left[\left(\omega_0-\omega\right) + \gamma_0\frac{\Delta P}{P_{th}}\frac{\left(\omega-\omega_0\right)\gamma_l + \left(\omega/2-\omega_l\right)\gamma_0}{\gamma_0\gamma_l - \left(\omega-\omega_0\right)\left(\omega/2-\omega_l\right)}\right].\end{aligned} \tag{22}$$

Below the threshold, the direction of radiation force is towards the nearest pressure antinode, if the bubble is driven below the resonance $\omega < \omega_0$, and towards a pressure node, if driven above resonance $\omega > \omega_0$. In order to assess the influence of the correction term (the second term in Eq. (22)) above the threshold, we note that the denominator of this expression can vanish at $\omega = \omega_\pm$:

$$\omega_\pm = \omega_l + \omega_0/2 \pm \sqrt{\left(\omega_l - \omega_0/2\right)^2 + 2\gamma_0\gamma_l}. \tag{23}$$

The fixed points of the dynamic system Eq. (10) are critical when the control parameters take the values $\omega = \omega_\pm$, $P = P_{th}(\omega_\pm)$ (neglecting the interaction in resonant triads). Here the confluence of all fixed points of this system takes place [22]. In the vicinity of these states the proposed approach is not applicable, and one should take into account the non-linear terms of higher order. The considered approach will be valid for the frequency interval, located not too close to the critical values $\omega_+ > \omega > \omega_-$. In this region, the denominator has a positive value. The numerator of the correction term vanishes at $\omega = \omega_* = (\omega_0\gamma_l + \omega_l\gamma_0)(\gamma_l + \gamma_0/2)^{-1}$. If $\omega_0 = 2\omega_l$, the reversal of the force direction (from attractive to repulsive and vice versa) occurs at exactly the same frequency at which it takes place below the threshold $\omega = \omega_0$. If $\omega_0 > 2\omega_l$, the change in the sign of the radiation force occurs at greater frequency than ω_0, and for $\omega_0 < 2\omega_l$ the change occurs at lower frequency than ω_0.

For a fixed frequency, the variation of the radiation force when one ignores the influence of the surface modes can be presented in the following form $F_z^{(0)} = F_z^{th}\left[1 + (\Delta P/P_{th})\right]^2 \approx F_z^{th}\left[1 + 2\,(\Delta P/P_{th})\right]$, where F_z^{th} is the value of the force at the threshold. Comparing this expression with the exact equation for the radiation force:

$$\begin{aligned} F_z &= F_z^{th}\left[1 + \left(\frac{\Delta P}{P_{th}}\right)\right]\frac{\sin\alpha_V}{\sin\alpha_V^{th}} \\ &= F_z^{th}\left[1 + \frac{\Delta P}{P_{th}}\left(1 + \frac{\gamma_0}{\omega_0 - \omega}\frac{(\omega-\omega_0)\gamma_l + (\omega/2 - \omega_l)\gamma_0}{\gamma_0\gamma_l - (\omega-\omega_0)(\omega/2-\omega_l)}\right)\right]. \end{aligned} \tag{24}$$

one can see that, for $\omega_0 = 2\omega_l$, accounting for the influence of the surface modes leads to a decrease in the magnitude of the force $F_z = F_z^{th}\big\{1 + (\Delta P/P_{th})\left[1 - \gamma_0\left(\gamma_l + \gamma_0/2\right)\left[\gamma_0\gamma_l - (\omega-\omega_0)(\omega/2-\omega_l)\right]^{-1}\right]\big\}$ in the entire frequency interval $\omega_- < \omega < \omega_+$. For $\omega_0 < 2\omega_l$ (or $\omega_0 > 2\omega_l$), the change in the sign of the force occurs at frequencies that do not coincide with ω_0. In the vicinity of these frequencies, the force can be less than in the hypothetical case, but the comparison itself does not make sense in these frequency domains.

Unfortunately there is currently no complete understanding of the implementation of various structures on the surface of the bubble. Only a few types of possible patterns have been observed at the specific values of the defining parameters [17, 56–58]. The rolls patterns were observed by Birkin *et al.* [57] at the pressure amplitude 24 Pa (zero-to-peak). The mean radius of the bubble was approximately 2.1 mm and the driving field had frequency of 1.500 kHz. The bubble was not in an infinite body of liquid, as the above theory assumes, but held under and against the end of a 6 mm diameter glass rod, which contained a small concave dimple to keep the bubble in place, which can in principle affect the bubble dynamics [24]. For this case, the characteristics of the bubble dynamics can be evaluated for the following values of the determining parameters: $\gamma = 1.4$ (polytropic exponent: air), $\sigma = 7.2 \times 10^2\,\mathrm{N\,m^{-1}}$ (surface tension: clean aqueous solution of salts in air, 20°C), $P_0 = 10^5$ Pa (ambient pressure), $\rho_0 = 988$ $\mathrm{kg\,m^{-3}}$ (equilibrium density liquid: water), $c = 1484\,\mathrm{m\,s^{-1}}$ (speed of sound in the liquid: water), $\nu = 10^{-6}\mathrm{m^2 s^{-1}}$ (kinematic viscosity liquid: water), $D = 2 \times 10^{-5}\mathrm{m^2 s^{-1}}$ (thermal diffusion coefficient liquid: water).

The frequency of monopole pulsations $\omega_0 = \sqrt{3\gamma\left(P_\infty + 2\sigma/R_0\right)\left(\rho_0 R_0^2\right)^{-1}}$ is set to $\omega_0/2\pi = f_0 = 1563$ Hz. The condition of the parametric resonance $\omega_0 \approx 2\omega_l$ is satisfied for $l = 14$ mode: $\omega_l = \sqrt{\sigma\left(l+1\right)\left(l+2\right)\left(l-1\right)\left(\rho_0 R_0^3\right)^{-1}}$, $\omega_{14}/2\pi = f_{14} = 789$ Hz. For comparison, the natural frequency of the nearest mode equals $\omega_{13}/2\pi = 709$ Hz. The damping factor for the breathing mode $\gamma_0 = \omega^2 R_0/2c + (2\nu/R_0^2) + 3(\gamma - 1)\left(\omega_0/2R_0\right)\left(D/2\omega\right)^{1/2}$ is the sum of radiation damping, viscous damping and damping owing to thermal diffusion, as estimated by a linear analysis. This factor is set to $\gamma_0 = (94.27 + 0.45 + 91.39) = 186.11$ $\mathrm{s^{-1}}$. The viscous damping of the l-th distortion mode, as estimated by a linear analysis, $\gamma_l = (l+2)(2l+1)\nu/R_0^2$, is set to $\gamma_{14} = 105.21$ $\mathrm{s^{-1}}$.

Figure 2 illustrates the excitation threshold for the generation of the $l = 14$ surface mode on the bubble wall and the location of the characteristic frequencies: f_-, f_0, $2f_{14}$, and f_+. The most likely candidate explanation for the discrepancy between this and the results of a laboratory experiment [57] (rolls pattern observed under driving with frequency of 1500 Hz and an amplitude of the acoustic signal 24 Pa) is the fact that the bubble was not free in the discussed experiment – the glass rod prevented its buoyant rise. The natural frequency of the tethered bubble is lower than that of a free bubble [59]. Moreover, the acoustic pressure near the rigid wall (glass) is higher than that measured by a hydrophone in the volume of liquid before insertion of the glass rod.

The behavior of the normalized volume amplitude, V_m/V_0, and $\sin\alpha_V$ versus frequency, $f = \omega/2\pi$, and pressure acting at the place of location of the bubble, $P_m = \rho_0\omega\varphi_m\cos(kd)$ are illustrated in FIG. 3 (a,b). The presence of the threshold appears as a break (a discontinuity in gradient indicated by a white line) on the surfaces shown in FIG. 3 (a, b). The dashed line at the panel (b) shows the contour where $\sin\alpha_V$ vanishes. The radiation force changes its sign at the corresponding values of the determining parameters $f = \omega/2\pi$ and P_m. Since for the case considered here we know that $\omega_0 < 2\omega_{14}$ $(1563 < 2 \times 789)$, the frequency at

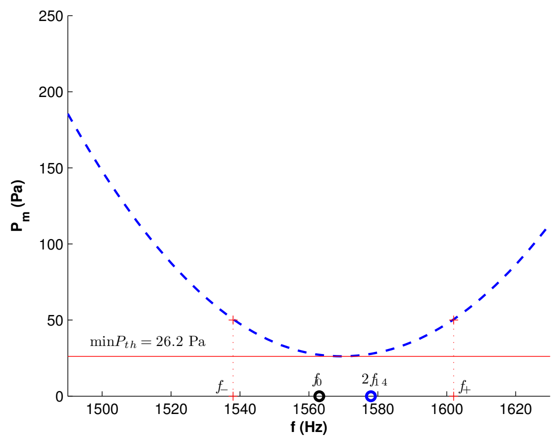

FIG. 2. (Color online) The control space for the acoustic pressure amplitude (P_m) and frequency ($f = \omega/2\pi$) of the pump field, as relating to an air bubble of equilibrium radius 2.1 mm in water under 1 atmosphere. The threshold curve for parametrically driven shape oscillations ($l = 14$, dashed curve) is shown. A horizontal line indicates a minimum of the threshold ($\min P_{th} = 26.2$ Pa). Location of the characteristic frequencies illustrates the closeness of parametric resonance $f_0 \approx 2f_{14}$ and the range of applicability of the current approach $f_- < f < f_+$.

which the sign changes decreases as the driving pressure increases above the threshold.

In the current study we have restricted ourselves to consideration of the simplest pattern which can be generated on the bubble wall (rolls). Extrapolation from these findings to the circumstances in which other patterns occur requires cumbersome calculations. The

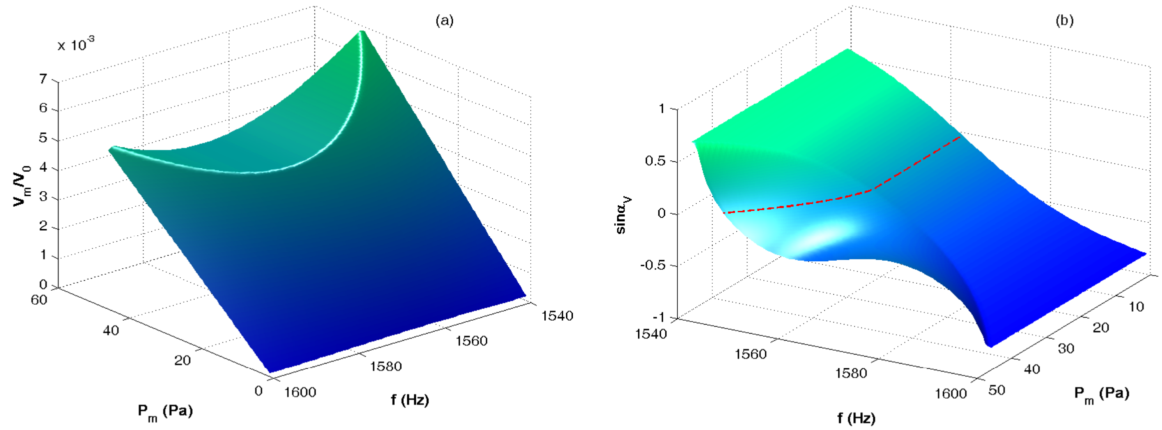

FIG. 3. (Color online) A surface plot of the normalized amplitude of the volume oscillations, V_m/V_0, (a). The two horizontal axes represent frequency, f, and the zero-to-peak amplitude of the external pressure field, P_m, acting in the place of bubble location. The variation of the $\sin\alpha_V$ determining the direction of the radiation force is shown at the panel (b). The dashed line illustrates the location of the contour where radiation force changes its direction.

form of the surface wave is important for a number of areas (e.g. the changes made during electrodeposition when bubbles with acoustically-activated surface waves are present on the electrode [57]). However this paper also focuses on the effect these surface waves have on the radiation force that determines the bubble's location. Acoustic fields have been used to levitate bubbles for decades [3, 60–63]. However the empirical observation that the bubble can 'dance' and 'shimmer' [64, 65] can be approached by understanding the effect that surface waves have on the radiation force. Because of this, and the applications that are facilitated by being able to use radiation forces to direct a bubble to a target area where the surface waves can perform a useful task (such as cleaning in crevices [66]), it is important to evaluate the static acoustic radiation torque [67, 68] on a parametrically distorted bubble.

A review of existing experiments (see supplement_materials_3.pdf [69]) has not identified any experimental set-up from the past when observations were taken under conditions, where variations in the strength of the radiation pressure above the threshold for parametric instability could occur. From our point of view, it is most easy to check the existence of these variations in determining the levitation position of the bubble in the conditions of the experiment described by Crum and Prosperetti [70], but using plain water instead of glycerol solution.

In an acoustic standing wave, bubbles can be levitated against the gravitation force of buoyancy by Bjerknes forces. Measurements of the pulsation amplitude of an individual gas bubble were made by acoustically levitating the air bubble near an antinode of an acoustic stationary wave [61, 70]. A bubble can be stably levitated if the Bjerknes and average buoyancy forces are equal. Thus:

$$\frac{\rho_0 g}{T}\int_0^T V(t)dt \approx \rho_0 g V_0 = (1/2)kP_m V_m \sin\alpha_V \sin(2kd). \tag{25}$$

A simple expression for the equilibrium levitation position of the bubble can be obtained provided one assumes the bubble is near the pressure antinode which usually implies that the size of the bubble is smaller than resonance. Under such circumstances, $\sin(kd) \approx kd$ and:

$$d = \frac{2\rho_0 g V_0}{k^2 P_m V_m \sin\alpha_V}. \tag{26}$$

For small driving pressures, the equilibrium position of the bubble is nearly inversely related to the square of drive pressure. However, as the driving pressures increased above the threshold for instability of the first distortion mode, the slope of the curve $d(P_m)$ will be changed according results presented in the current paper. Moreover, as soon as the amplitude of the external oscillating pressure exceeds the threshold for the excitation of the surface mode that has a driving pressure threshold that is higher than, but closest to, that of the Faraday wave mode (this is usually the one that has a mode number that is one integer higher than the mode number of the Faraday wave), it will become difficult to determine the levitation position since the bubbles demonstrate the erratic "dancing" motion. This translation instability is caused by shape oscillations.

V. CONCLUSION

The variations in the acoustic radiation pressure exerted by a standing sound wave on a gas bubble above the threshold for generation of surface modes have been studied theoretically. In the framework of a simple model, we were able to reveal how the nonlinear interactions between breathing and distortion modes affect the magnitude and direction of the radiation force. It has been shown that the growth of the radiation force with increasing amplitude of the acoustic wave above the threshold slows down and the frequency at which this force changes its sign is shifted.

ACKNOWLEDGMENTS

The contribution of AOM was supported by POI FEBRAS (project no 117030110034-7). The contribution of TGL was supported by EPSRC grant EP/M027260/1. The data supporting this study are openly available as DOI: XXXX from the University of Southampton repository at http://dx.doi.org/XXXX (XXXX to be replaced by details once paper is accepted, in line with Repository policy).

---

[1] K. Yosioka and Y. Kawasima, "Acoustic radiation pressure on a compressible sphere," Acustica **5**, 167–173 (1955).

[2] P. Gor'kov, "On the forces acting on a small particle in an acoustic field in an ideal fluid," Sov. Phys. Dokl. **6**, 773–775 (1962).

[3] A. Eller, "Force on a bubble in a standing acoustic wave," J. Acoust. Soc. Am. **43**, 170–171 (1968).

[4] P. Lee and T. G. Wang, "Acoustic radiation force on a bubble," J. Acoust. Soc. Am. **93**, 1637–1640 (1993).

[5] A. A. Doinikov, "Acoustic radiation force on a spherical particle in a viscous heat-conducting fluid. I. General formula," J. Acoust. Soc. Am. **101**, 713–721 (1997).

[6] A. A. Doinikov, "Acoustic radiation pressure on a compressible sphere in a viscous fluid," J. Fluid Mech. **267**, 1–21 (1994).

[7] A. A. Doinikov, "On the radiation pressure on small spheres," J. Acoust. Soc. Am. **100**, 1231–1233 (1996).

[8] A. Doinikov, "Acoustic radiation force on a bubble: Viscous and thermal effects," J. Acoust. Soc. Am. **103**, 143–147 (1998).

[9] J. T. Karlsen and H. Bruus, "Forces acting on a small particle in an acoustical field in a thermoviscous fluid," Phys. Rev. E **92**, 043010 (2015).

[10] A. I. Eller and L. A. Crum, "Instability of the Motion of a Pulsating Bubble in a Sound Field," J. Acoust. Soc. Am. **47**, 762–767 (1970). doi: http://dx.doi.org/10.1121/1.1911956

[11] R. K. Gould, "Recified diffusion in the presence of, and absence of, acoustic streaming," J. Acoust. Soc. Am. **56**, 1740–1746 (1974). doi: http://dx.doi.org/10.1121/1.1903506

[12] C. Hullin, “Pulsieren de luftblasen in wasser,” Acustica **37**, 64–72 (1977).

[13] A. D. Phelps and T. G. Leighton, “High-resolution bubble sizing through detection of the subharmonic response with a two-frequency excitation technique,” J. Acoust. Soc. Am. **99**, 1985–1992 (1996). (doi:10.1121/1.415385)

[14] T. G. Leighton, D. G. Ramble, and A. D. Phelps, “The detection of tethered and rising bubbles using multiple acoustic techniques,” J. Acoust. Soc. Am. **101**, 2626–2635 (1997). (doi:10.1121/1.418503)

[15] D. Ramble, A. Phelps, and T. G. Leighton, T. G. “On the relation between surface waves on a bubble and the subharmonic combination-frequency emission,” Acta Acustica **84**, 986–988 (1998).

[16] E. Trinh, D. Thiessen, and R. Holt, “Driven and freely decaying nonlinear shape oscillations of drops and bubbles immersed in a liquid: experimental results,” J. Fluid Mech. **364**, 253–272 (1998). (doi:10.1017/S0022112098001153)

[17] Y. E. Watson, P. R. Birkin, and T. G. Leighton, “Electrochemical detection of bubble oscillation,” Ultrason. Sonochem. **10**, 65–69 (2003). (doi:10.1016/S1350-4177(02)00149-9)

[18] R. Dangla and C. Poulain, “When sound slows down bubbles,” Phys. Fluids **22**, 041703 (2010). (doi:10.1063/1.3415496)

[19] M. Versluis, D. E. Goertz, P. Palanchon, I. L. Heitman, S. M. van der Meer, B. Dollet, N. de Jong, and D. Lohse, “Microbubble shape oscillations excited through ultrasonic parametric driving,” Phys. Rev. E **82**, 026321 (2010). (doi:10.1103/PhysRevE.82.026321)

[20] F. Prabowo and C. D. Ohl, “Surface oscillation and jetting from surface attached acoustic driven bubbles,” Ultrason. Sonochem. **18**, 431–435 (2011). (doi:10.1016/j.ultsonch.2010.07.013)

[21] X. Xi, F. Cegla, R. Mettin, F. Holsteyns, A. Lippert, “Study of non-spherical bubble oscillations near a surface in a weak acoustic standing wave field,” J. Acoust. Soc. Am. **135**, 1731–1741 (2014). (doi:10.1121/1.4864461)

[22] A. O. Maksimov and T. G. Leighton, “Transient processes near the acoustic threshold of parametrically-driven bubble shape oscillations,” Acta acustica **87**, 322–332 (2001).

[23] A. O. Maksimov, T. G. Leighton, and P. R. Birkin, “Self focusing of acoustically excited Faraday ripples on a bubble wall,” Phys. Lett. A. **372**, 3210–3216 (2008).

[24] A. O. Maksimov and T. G. Leighton, "Pattern formation on the surface of a bubble driven by an acoustic field," Proc. R. Soc. A **468**, 57–75 (2012).

[25] T. J. Asaki and P. L.Marston, "Acoustic radiation force on a bubble driven above resonance," J. Acoust. Soc. Am. **96**, 3096–3099 (1994). (doi: http://dx.doi.org/10.1121/1.411246)

[26] T. J. Asaki and P. L. Marston, "Free decay of shape oscillations of bubbles acoustically trapped in water and sea water," J. Fluid Mech. **300**, 149–167 (1995). (https://doi.org/10.1017/S0022112095003648)

[27] T. J. Asaki and P. L. Marston, "The effect of a soluble surfactant on quadrupole shape oscillations and dissolution of air bubbles in water," J. Acoust. Soc. Am. **102**, 3372–3377 (1997). (doi: http://dx.doi.org/10.1121/1.421007)

[28] R. G. Holt, "Faraday waves and ultrasonic foggers," J. Acoust. Soc. Am. **121**, 3114 (2007). (doi: http://dx.doi.org/10.1121/1.4808517)

[29] P. Moriarty and R. G. Holt, "Faraday waves produced by periodic substrates: Mimicking the alligator water dance," J. Acoust. Soc. Am. **129**, 2411 (2011). (http://dx.doi.org/10.1121/1.3587858)

[30] T. G. Leighton, "The acoustic bubble: Oceanic bubble acoustics and ultrasonic cleaning," Proceedings of Meetings on Acoustics (POMA), Acoustical Society of America, **24**, 070006 (2015). (http://dx.doi.org/10.1121/2.0000121; http://resource.isvr.soton.ac.uk/staff/pubs/PubPDFs/POMA%20Pruac%202015.pdf)

[31] P. R. Birkin, D. G. Offin, T. G. Leighton, "An activated fluid stream – New techniques for cold water cleaning," Ultrason. Sonochem. **29**, 612–618 (2016).

[32] T. G. Leighton, "The acoustic bubble: Ocean, cetacean and extraterrestrial acoustics, and cold water cleaning," J. Phys.: Conf. Ser. **797**, 012001 (2017). (doi:10.1088/1742-6596/797/1/012001; https://www.researchgate.net/publication/312510609)

[33] P. R. Birkin, D. G. Offin, C. J. B. Vian, R. P. Howlin, J. I. Dawson, T. J. Secker, R. C. Herve, P. Stoodley, R. O. C. Oreffo, C. W. Keevil and T. G. Leighton, "Cold water cleaning of brain proteins, biofilm and bone - harnessing an ultrasonically activated stream," Phys. Chem. Chem.Phys. **17**, 20574–20579 (2015). (doi: 10.1039/C5CP02406D)

[34] R. P. Howlin, S. Fabbri, D. G. Offin, N. Symonds, K. S. Kiang, R. J. Knee, D. C. Yoganantham, J. S. Webb, P. R. Birkin, T. G. Leighton and P. Stoodley, "Removal of dental biofilms with a novel ultrasonically-activated water stream," J. Dental Research **94**(9), 1303–1309 (2015).

(doi:10.1177/0022034515589284)

[35] P. R. Birkin, D. G. Offin, C. J. B. Vian and T. G. Leighton, “Electrochemical ”bubble swarm” enhancement of ultrasonic surface cleaning,” Phys. Chem. Chem. Phys. **17**(33), 21709–21715 (2015). (doi:10.1039/c5cp02933c)

[36] M. Salta, L. Goodes, B. Mass, S. Dennington, T. Secker, T. G. Leighton, “Bubbles vs. biofilms: A novel method for the removal of marine biofilms attached on antifouling coatings using an ultrasonically activated water stream,” Surf. Topogr.: Metrol. Prop. **4**(3), 034009 (2016). (doi: 10.1088/2051-672X/4/3/034009)

[37] L. Goodes, T. Harvey, N. Symonds and T. G. Leighton, “A comparison of ultrasonically activated water stream and ultrasonic bath immersion cleaning of railhead leaf-film contaminant,” Surf. Topogr.: Metrol. Prop. **4**(3), 034004 (2016). (doi: 10.1088/2051-672X/4/3/034004)

[38] T. G. Leighton, “Climate Change, Dolphins, Spaceships and Antimicrobial Resistance – the Impact of Bubble Acoustics,” Proceedings of 24th International Congress on Sound and Vibration ICSV24 (23–27 July 2017, London), paper KL5, pp. 1–16.

[39] L. D. Landau and E. M. Lifshitz, *Fluid Mechanics* (Pergamon Press, Oxford, 1966), pp. 281–285.

[40] L. Zhang and P. L. Marston, “Axial radiation force exerted by general non-diffracting beams,” J. Acoust. Soc. Am. **131**, EL329–El335 (2012). (doi: 10.1121/1.3693387)

[41] L. A. Crum, “Bjerknes forces on bubbles in a stationary sound field,” J. Acoust. Soc. Am. **57**, 1363–1370 (1975).

[42] T. G. Leighton, A. J. Walton and M. J. W. Pickworth, “Primary Bjerknes forces,” European Journal of Physics. **11**, 47–50 (1990).

[43] A. Francescutto and R. Nabergoj, “Pulsation amplitude threshold tor surface waves on oscillating bubbles,” Acustica. **41**, 215–220 (1978).

[44] M. S. Longuet-Higgins, “Monopole emission of sound by asymmetric bubble oscillations. 1. Normal modes,” J. Fluid Mech. **201**, 525–541 (1989). (doi:10.1017/S0022112089001035)

[45] M. S. Longuet-Higgins, “Monopole emission of sound by asymmetric bubble oscillations. 2. An initial value problem,” J. Fluid Mech. **201**, 543–565 (1989) (doi:10.1017/S0022112089001047)

[46] C. C. Mei and X. Zhou, “Parametric resonance of a spherical bubble,” J. Fluid Mech. **229**, 29–50 (1991). (doi:10.1017/S0022112091002926)

[47] T. J. Asaki, P. L. Marston, and E. Trinh, "Shape oscillations of bubbles in water driven by modulated ultrasonic radiation pressure: observation and detection with scattering laser light," J. Acoust. Soc. Am. **93**, 706–713 (1993). (doi:10.1121/1.405434)

[48] Z. Feng and L. Leal, "Nonlinear bubble dynamics," Annu. Rev. Fluid Mech. **29**, 201–247 (1997). (doi:10.1146/annurev.fluid.29.1.201)

[49] A. O. Maksimov, "Hamiltonian description of bubble dynamics," J. Exp. Theor. Phys. **106**, 355–370 (2008). (doi:10.1134/S1063776108020143)

[50] See supplementary material at [URL will be inserted by AIP] for the form of governing equations for the amplitudes of interacting modes. The file entitled 'SuppPub1.pdf' is contained within the Electronic Supplement No. 1: A. Maksimov and T. G. Leighton, Electronic supplementary material to "Acoustic radiation force on parametrically distorted bubble,"(2017). The University of Southampton electronic data repository http://dx.doi.org/ 10.5258/SOTON/to-be-inserted-if-accepted.

[51] M. C. Cross and P. C. Hohenberg, "Pattern formation outside of equilibrium," Rev. Mod. Phys. **65**, 851–1123 (1993). (doi:10.1103/RevModPhys.65.851)

[52] S. Wiggins, *Introduction to applied nonlinear dynamical systems and chaos*, (Springer Verlag, New York, 1996), pp. 193–210.

[53] L. Zhang, P. L. Marston, "Acoustic radiation force expressed using complex phase shifts and momentum-transfer cross sections," J. Acoust. Soc. Am. **140**, EL178–EL183 (2016). (doi: 10.1121/1.4959966)

[54] P. L. Marston, L. Zhang,"Relationship of scattering phase shift to special radiation force conditions for spheres in axisymmetric wave-field," J. Acoust. Soc. Am. **141**, 3042–3049 (2017). (doi: 10.1121/1.4982203)

[55] See supplementary material at [URL will be inserted by AIP] for the scattering phase shift for parametrically distorted bubble. The file entitled 'SuppPub2.pdf' is contained within the Electronic Supplement No. 2: A. Maksimov and T. G. Leighton, Electronic supplementary material to "Acoustic radiation force on parametrically distorted bubble,"(2017). The University of Southampton electronic data repository http://dx.doi.org/ 10.5258/SOTON/to-be-inserted-if-accepted.

[56] P. R. Birkin, Y. E. Watson, T. G. Leighton, "Efficient mass transfer from an acoustically oscillated gas bubble," J. Chem. Soc. Chem. Commun. **24**, 2650–2651 (2001).

(doi:10.1039/B107616G)

[57] P. R. Birkin, Y. E. Watson, T. G. Leighton, and K. L. Smith, "Electrochemical detection of Faraday waves on the surface of a gas bubble," Langmuir **18**, 2135–2140 (2002). (doi:10.1021/la0111001)

[58] P. R. Birkin, D. G. Offin, C. J. B. Vian, T. G. Leighton, and A. O. Maksimov, "Investigation of non-inertial cavitation produced by an ultrasonic horn," J. Acoust. Soc. Am. **130**, 3297–3308 (2011). (doiI: 10.1121/1.3650537)

[59] A. O. Maksimov, "On the volume oscillations of a tethered bubble," J. Sound Vib. **283**, 915–926 (2005).

[60] L. A. Crum and A. I. Eller, "The motion of air bubbles in stationary sound field," J. Acoust. Soc. Am. **48**, 181–189 (1970).

[61] T. J. Matula, A. M. Cordry, R. A. Roy, and L. A. Crum, "Bjerknes force and bubble levitation under single-bubble sonoluminescence conditions," J. Acoust. Soc. Am. **102**, 1522–1527 (1997).

[62] R. G. Holt and L. A. Crum, "Acoustically forced oscillations of air bubbles in water: Experimental results," J. Acoust. Soc. Am. **91**, 1924–1932 (1992). (doi.org/10.1121/1.403703)

[63] R. G. Holt and D. F. Gaitan, "Observation of stability boundaries in the parameter space of single bubble sonoluminescence," Phys. Rev. Lett. **77**, 3791–3794 (1996).

[64] T. G. Leighton, *The Acoustic Bubble*, (Academic Press, London, 1994), pp. 415–419.

[65] J. Ellenberger, R. Krishna, "Levitation of air bubbles in liquid under low frequency vibration excitement," Chemical Engineering Science. **62**, 5669–5673 (2007).

[66] D. G. Offin, P. R. Birkin, and T. G. Leighton, "An electrochemical and high-speed imaging study of micropore decontamination by acoustic bubble entrapment," Phys. Chem. Chem. Phys. **16**, 4982–4989 (2014). (doi:10.1039/C3CP55088E)

[67] Z. W. Fan, D. Q. Mei, K. Y. Yang, and Z. C. Chen, "Acoustic radiation torque on an irregular shaped scatterer in an arbitrary sound field," J. Acoust. Soc. Am. **124**, 27277–2732 (2008).

[68] L. Zhang and P. L. Marston, "Acoustic radiation torque and the conservation of angular momentum," J. Acoust. Soc. Am. **129**, 1679–1680 (2011).

[69] See supplementary material at [URL will be inserted by AIP] for the comparison with experiment. The file entitled 'SuppPub3.pdf' is contained within the Electronic Supplement No. 3: A. Maksimov and T. G. Leighton, Electronic supplementary material to "Acoustic radiation

force on parametrically distorted bubble,"(2017). The University of Southampton electronic data repository http://dx.doi.org/ 10.5258/SOTON/to-be-inserted-if-accepted.

[70] L. A. Crum, A. Prosperetti, "Nonlinear oscillations of gas bubbles in liquids: An interpretation of some experimental results," J. Acoust. Soc. Am. **73** 121–127 (1983).

[71] L. I. Schift, *Quantum Mechanics*, 3^{rd} ed. (McGraw-Hill, New York, 1968), pp. 131–133.

[72] P. R. Birkin, D. G. Offin, C. J. B. Vian, T. G. Leighton, A. O. Maksimov, "Investigation of noninertial cavitation produced by an ultrasonic horn," J. Acoust. Soc. Am. **130**, Pt. 2, 32973308 (2011).

[73] Y. Hao, A. Prosperetti, "The effect of viscosity on the spherical stability of oscillating gas bubbles," Phys. Fluids **11**, 1309–1317 (1999).

[74] M. Guedra, C. Inserra, C. Mauger, and B. Gilles, "Experimental evidence of nonlinear mode coupling between spherical and nonspherical oscillations of microbubbles," Phys. Rev. E **94**, 053115 (2016).

[75] X. Xi, F. B. Cegla, M. Lowe, A. Thiemann, T. Nowak, R. Mettin, F. Holsteyns, A. Lippert, "Study on the bubble transport mechanism in an acoustic standing wave field," Ultrasonics **51**, 1014–1025 (2011).

References [71–75] are additional items cited in the Supplements.

FIGURE CAPTIONS

Fig. 1 (Color online) Schematic of a parametrically distorted bubble in the field of a standing acoustical wave φ_{in} of the frequency ω with d being the distance between the equilibrium center of the bubble and the nearest plane of the velocity nodes (or potential antinodes). The size of the bubble is assumed to be smaller than the acoustic wavelength λ, thus, there is a region around the bubble, which may be regarded as incompressible.

Fig. 2 (Color online) The control space for the acoustic pressure amplitude (P_m) and frequency ($f = \omega/2\pi$) of the pump field, as relating to an air bubble of equilibrium radius 2.1 mm in water under 1 atmosphere. The threshold curve for parametrically driven shape oscillations ($l = 14$, dashed curve) is shown. A horizontal line indicates a minimum of the threshold ($\min P_{th} = 26.2$ Pa). Location of the characteristic frequencies illustrates the closeness of parametric resonance $f_0 \approx 2f_{14}$ and the range of applicability of the current approach $f_- < f < f_+$.

Fig. 3 (Color online) A surface plot of the normalized amplitude of the volume oscillations, V_m/V_0, (a). The two horizontal axes represent frequency, f, and the amplitude of the external pressure field, P_m, acting in the place of bubble location. The variation of the $\sin\alpha_V$ determining the direction of the radiation force is shown at the panel (b). The dashed line illustrates the location of the contour where radiation force changes its direction.

Click here to access/download
Supplemental Files for Publication
SuppPub1.pdf